International Journal of Multiphase Flow 65 (2014) 117–126

Contents lists available at ScienceDirect

International Journal of Multiphase Flow

journal homepage: www.elsevier.com/locate/ijmulflow

Spectral density analysis of the interface in stratified oil–water flows

A.H. Barral, P. Angeli *

Department of Chemical Engineering, University College London, London, United Kingdom

ARTICLE INFO

Article history:
Received 11 October 2013
Received in revised form 29 May 2014
Accepted 3 June 2014
Available online 23 June 2014

Keywords:
Stratified oil–water flow
Power spectrum
FFT
Conductance probe

ABSTRACT

In this work the wavy interface of stratified oil–water flows was investigated using wire conductance probes. The experiments were carried out in a 38 mm ID acrylic pipe using water and oil (Exxsol D140 oil: $\rho_o = 830$ kg m^{-3}, $\mu_o = 0.0055$ kg m^{-1} s^{-1}) as test fluids. High-speed imaging revealed that almost two-dimensional interfacial waves develop at the inlet junction for input oil-to-water flow rate ratios different from one. Downstream the inlet section, however, the interface has a complex three dimensional structure with very small amplitude contributions. The structure of such interfaces can be properly investigated from the power spectrum of the conductance probe signal. A rigorous and detailed methodology is presented for estimating the power spectrum of the interface signal that is based on the Wiener–Khinchine theorem and makes extensive use of a Fast Fourier Transform (FFT) algorithm. Interface spectra were studied at two locations, close to the inlet of the test section and at 7 m downstream. The results showed that the waves at the inlet have a unique peak frequency of about 19 Hz and that, at the downstream location, this frequency is still present but has a smaller significance compared to that caused by the mechanical vibrations of the set up. This frequency was independent of the flow rates and could be a characteristic of the pair of the test fluids used rather than of the flow.

1. Introduction and background

The simultaneous flow of two fluids in a pipe (either liquid–liquid or gas–liquid) occurs in a large number of applications in the energy, oil and process industries. Different flow patterns can develop depending on flow parameters such as mixture velocity and input flow rate ratio, properties of the fluids (density, viscosity and surface tension) and the pipe size and inclination. The type of flow pattern determines important parameters of the two-phase flow (such as pressure drop, heat and mass transfer coefficients) and has an effect on the design and operation of multiphase pipelines.

The shape and characteristics of the interface during the stratified flow of oil–water mixtures in horizontal or slightly inclined pipes have been the object of many investigations. In general, it is assumed that the flow would generate interfacial waves which, depending on the conditions, could become unstable and grow in amplitude. From these waves, drops would form and detach. This description was generally drawn from results in gas–liquid systems (see, for example, the five mechanisms of drop formation in gas–liquid flow in Ishii and Grolmes, 1975). The appearance of drops in stratified flows defines the onset of transition towards other flow regimes and, therefore, the study of interfacial structures is important for understanding the mechanism of transition to other patterns. These transitions have been discussed in e.g. Trallero (1995), Al-Wahaibi and Angeli (2007), Al-Wahaibi et al. (2007).

To study wave structures researchers have been using transparent (acrylic or glass) test pipes coupled with high-speed imaging. The benefits of such techniques, however, depend on the existence of visually identifiable waves. Oliemans (1986), Bai (1995), Bannwart (1998), Rodriguez and Bannwart (2006) studied wave characteristics in annular flows of heavy viscous oil and water from images, where defined wavy structures could be followed and investigated. Similarly, Al-Wahaibi and Angeli (2011) investigated the characteristics of oil–water flows from visual inspection and analysis of images using low-viscosity oil. Our previous studies with this oil, however, showed that almost two-dimensional waves appeared only at the inlet of the test section for input oil-to-water flow rate ratios different from 1. In contrast, further downstream the test section and at the inlet for input ratios close to 1 the oil–water interface did not show any easily identifiable waves. Instead the interface appeared to be fluctuating with small three-dimensional perturbations (Barral and Angeli, 2013). Such interface shapes make very difficult the quantitative analysis of wave characteristics via imaging, even when complex mathematical treatments are used. De Castro et al. (2012) investigated stratified

* Corresponding author. Tel.: +44 (0) 20 7679 3832.
E-mail address: p.angeli@ucl.ac.uk (P. Angeli).

http://dx.doi.org/10.1016/j.ijmultiphaseflow.2014.06.005
0301-9322/

oil–water flows with viscous oil (0.3 Pas). They identified interfacial waves and classified them in three groups according to size using high-speed imaging. They further employed Fourier filters to treat the images and allow for graphical analysis. Although the authors were able to report wave lengths and amplitudes, this procedure required a large simplification, as only the so-called intermediate waves were filtered in for analysis.

A different approach for the study of the fluctuating three dimensional structure of the interface was presented in a previous work by Barral and Angeli (2013) via the use of a double wire conductance probe. The use of conductance probes (including double-wire ones) has been extensive for over 50 years in both gas–liquid and liquid–liquid flows and in a variety of applications (Jurman et al., 1989; Tsochatzidis et al., 1992; Andritsos 1992; Azzopardi 1997; Fossa 1998; Wu and Ishii 1999; Kim et al. 2000; Wang et al., 2004; Chakrabarti et al., 2006; Panagiotopoulos et al., 2007; Alamu and Azzopardi 2011; Xu et al., 2012; Zhai et al., 2012; to name just a few). More recently, several investigators have attempted to identify flow patterns in oil–water flows by analyzing conductance probe signals, for example Hernández et al. (2006), Jin et al. (2003), Sun et al. (2011), Du et al. (2012). Given the complexity of such flows, including many non-stratified patterns, the authors needed to use complex mathematical techniques in order to deal, in many cases, with non-stationary data.

It has been found previously that the records of the interface height over time collected with a double wire conductance probe in horizontal stratified oil–water flows are stationary and follow a Gaussian distribution (Barral and Angeli, 2013). These properties allowed the estimation of the time-average interface height and related time average flow parameters (such as in-situ water fraction and actual velocities of the two phases) with confidence intervals. Under these conditions the power spectrum of the interface signal could be estimated via the Wiener–Khinchine theorem and some results were presented from the direct computation of the auto-correlation function. In this present work, the calculation of the power spectrum of the probe signal is thoroughly investigated; improvements based on windowing and truncation and corrections related to the circular convolution problem are introduced. A complete methodology widely applicable to stratified flows is presented to perform the spectral analysis of the oil–water interface signal, based on the extensive use of the Fast Fourier Transform (FFT). Following this procedure, the contributing frequencies in the wavy interface are identified close to the inlet of the test section and further downstream the inlet for different oil and water flow rates.

2. Experimental set-up and data acquisition

Experiments were performed in the oil–water flow facility located in the Department of Chemical Engineering, UCL. The rig consists of a 38 mm ID acrylic test pipe, which allows the visual inspection of the flow. The test fluids used are tap water ($\rho = 1000\ \mathrm{kg\ m^{-3}}$ and $\mu = 0.001\ \mathrm{kg\ m^{-1}\ s^{-1}}$) and ExxsolD140 oil ($\rho = 830\ \mathrm{kg\ m^{-3}}$ and $\mu = 0.0055\ \mathrm{kg\ m^{-1}\ s^{-1}}$), where ρ and μ are density and viscosity, respectively. The two fluids are stored and pumped separately using centrifugal pumps. Their flow rates are regulated via gate valves and measured separately with variable area flow meters (ABB Instrumentation Ltd.) with a range from 20 L $\mathrm{min^{-1}}$ to 250 L $\mathrm{min^{-1}}$ and 1% FS accuracy. The flow rate values are logged in a computer at a high sampling frequency (i.e. 256 Hz).

Oil and water are joined at a Y-shaped inlet section, with the top duct (oil) inclined 10° downwards and the bottom one (water) kept horizontal. Both ducts are 38 mm ID and made of acrylic (Fig. 1). This junction allows the two fluids to enter the test pipe in layers

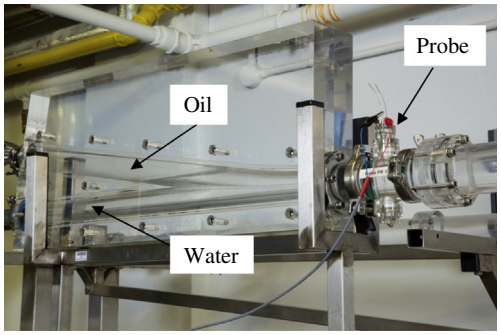

Fig. 1. Photograph of the *Y*-inlet section and one of the probes installed at Position 1.

according to their density, minimizing mixing. There is no additional split plate. The test pipe consists of two horizontal sections, each 8 m long, joined with two 90° elbows. After the test section, the mixture of the two fluids flows into a separator vessel equipped with a KnitMesh™ coalescer. Oil and water are then returned from the top and the bottom of the separator respectively into their storage tanks. A high speed video camera (Phantom Miro 4) was used to record the flow patterns and to inspect the oil–water interface along the pipe.

2.1. Double wire conductance probe

Two double wire conductance probes were used in the present work for the investigations of the oil–water interface structure. The probes consist of two parallel stainless steel wires, 0.5 mm in diameter, located either 2 mm apart (probe 1) or 5 mm apart (probe 2), and stretched along the vertical pipe diameter. Fig. 2 shows a photograph of the 2 mm probe; the 5 mm probe is identical, apart from the distance between the wires.

The probes were located either immediately after the inlet section or further downstream the pipe at about 7 m from the inlet (~180 *D*) where the flow is assumed to be fully developed. In the experiments one probe was used (either the 2 mm or the 5 mm) but some experiments were also carried out with both probes installed at the different locations. In the latter case, the 5 mm probe was placed close to the inlet and the 2 mm one in the

Fig. 2. Photograph of the 2-mm double-wire, conductance probe.

downstream location. In a large number of trials it was found that the probes gave the same spectra when used at the same location under the same oil–water flow rates. No other instrumentation was placed before or between the probes, in order to minimize flow disturbances. It was confirmed that, when both probes were present, the first probe did not affect the signal of the second one. In the presentation of the results, the type, number and location of the probes are clearly given.

During stratified oil–water flow, the probe signal provides a measurement of the interface height variations over time. The impedance of the overall set-up is designed to be negligible (i.e. all resistance is due to conductance). The signal was related to interface height through an off-line calibration procedure where air was used instead of oil, as they are both non-conductive. The probe signal was found to give a linear response against the water interface height. A calibration curve was developed for each conductance probe. Calibrations were repeated after cleaning operations or when required.

2.2. Data acquisition and pre-treatment

The conductance probe data was initially treated as detailed in Barral and Angeli (2013) to remove any spurious trends that could be introduced by the acquisition system and compensate for differences in temperature and water salinity. The signal was collected at 256 Hz over 4 min, which was found to give stationary and Gaussian records at 90% confidence level; these properties allow the spectral analysis of the data via the Wiener–Khinchine theorem. The calculation of the signal power spectrum is discussed below.

3. Power spectrum estimate

The power spectrum of the wavy interface signal has been estimated by the extensive use of the Fast Fourier Transform algorithm (FFT), as shown in the following sections. From inspection of the spectrum, information about the flow, such as the distribution and relative importance of contributing frequencies, and the average power can be obtained. It is worth mentioning here that the procedure for estimating the power spectrum is not a direct application of FFT to the probe data, but it is built from robust information on the statistical structure of the signal. The spectrum obtained from a simple FFT of the oil–water interface signal data is often noisy and unclear, and might include artefacts from the algorithm that cannot be evaluated and may lead to spurious results.

3.1. The Fast Fourier Transform algorithm (FFT)

The Fourier Transform of a given signal in time, $x(t)$, can be obtained from the solution of an improper integral that brings the signal into the frequency domain, $X(f)$. However, in most practical applications, the available data is a sample of discrete values collected over a finite interval of time, as it is the case of the current experimental data obtained with the conductivity probe (i.e. sampling at 256 Hz over 4 min). A discrete substitute to the Fourier Transform operation is therefore required. Furthermore, the substitute must uniquely represent the fluctuations of the interface regardless of the sample size. This can be ensured by applying the Sampling Theorem (Shannon, 1949). In the present study, preliminary spectra of oil–water flows showed small contributions at frequencies larger than 60 Hz and, according to the theorem, the choice of 256 Hz as sampling frequency is justified.

The calculation of the discrete Fourier Transform may require significant computation memory and time, especially when treating large data records. In practice, commercial software offers the possibility of computing the discrete Fourier Transform via simple built-in algorithms, known as the Fast Fourier Transform (FFT) algorithms, generally in use for almost 50 years (Cooley and Tuckey, 1965). The FFT is a powerful tool suitable for the estimation of the power spectrum, but must be applied carefully depending on the particular data to be analyzed. In this investigation, a direct computation of the discrete Fourier Transform has been compared against results obtained via the FFT command in MatLab. Both calculations gave identical spectra and the MatLab command was subsequently used in the calculation of Fourier Transforms.

3.2. Statistical properties of the oil–water interface data

All records analyzed in this work have been verified to be stationary and Gaussian, using the method of Reverse Arrangements and applying a Chi-Square goodness-of-fit test with 12 class intervals and 3 degrees of freedom, respectively (Barral and Angeli, 2013). Further, q–q plots and graphs of both experimental and Gaussian cumulative density functions have been compared to validate the procedure and confirm the Gaussian behavior.

Additionally, the data collected was found to be ergodic. Ergodicity is a further property of stationary records that ensures that one sample is representative of the process (Bendat and Piersol, 2010). Furthermore, the time-averaged estimate of the auto-correlation function of an ergodic record is known to be equal to the theoretical auto-correlation function of the process (Auñón and Chandrasekar, 1997). This feature allows the computation of the power spectrum of stratified, oil–water finite samples of data via the auto-correlation function, as explained below.

3.3. Procedure to estimate the power spectrum

According to the Wiener–Khinchine theorem the two-sided power spectrum of a time-series record in the frequency domain (i.e. includes positive and negative frequencies) equals the Fourier Transform of the auto-correlation function of the record, as long as the record is stationary and follows a Gaussian distribution. Mathematically, the theorem is expressed as follows:

$$S(f) = \int_{-\infty}^{+\infty} R_h(\tau) e^{-j2\pi f\tau} d\tau \tag{1}$$

where $S(f)$ is the two-sided power spectrum in the frequency domain, τ represents time delay and $R_h(\tau)$ is the auto-correlation function for a given time delay. Since the record is stationary and ergodic, Eq. (1)can be time-limited so that only the 4 min sampling time is considered, and the spectrum obtained will be the complete process spectrum:

$$S(f) = \int_{0}^{T} R_h(\tau) e^{-j2\pi f\tau} d\tau \tag{2}$$

where T is the sampling time, equal to 4 min.

The auto-correlation function is an *even* function, which is an important property. If the integrand of Eq. (1)is expanded using Euler's relationship, the imaginary part (the sin function, *odd*) will vanish, because the improper integral of the product of an even and an odd function is 0. As a consequence, the power spectrum turns out to be the Fourier cosine transform of the auto-correlation function. Because of that, the power spectrum is a *positive*, *real* and *even* function of the frequency. The last property (i.e. even function) explains why the power spectrum is the mirror image of itself with respect to the Nyquist frequency.

Eq. (2)can be discretized and provides a way to estimate the power spectrum of the interface of oil–water flows as long as a

time-averaged estimate of the auto-correlation function is calculated. This is defined as (Auñón and Chandrasekar, 1997):

$$R_h(\tau) = \lim_{T\to\infty} \frac{1}{2T} \int_0^T h(t)h(t+\tau)dt \quad (3)$$

where $h(t)$ is the instantaneous value of interface height collected at time t, between 0 and T; τ represents the time delay.

Generally, there are two main groups of alternative procedures to estimate the auto-correlation function in Eq. (3), either via direct discretization and computation of the equation, or via the FFT algorithm. Barral and Angeli (2013) provided preliminary results using the first procedure, but the second approach is usually more convenient than the direct computation because it is significantly faster. During this investigation, auto-correlation estimates of the signal from the oil–water interface were calculated directly from Eq. (3)and also via two procedures involving FFT (ensemble average and periodogram methods, Auñón and Chandrasekar, 1997). It was found that the spectra calculated from the three approaches were qualitatively equivalent. The method selected uses extensively the FFT and is based on the resemblance of the time-averaged auto-correlation function (Eq. (3)) and the convolution of the time signal, $h(t) * h(t)$:

$$h(t)^* h(t) = \int_{-\infty}^{+\infty} x(\tau)x(t+\tau)d\tau \quad (4)$$

The Convolution Theorem establishes that the convolution operation between two signals in the time domain, $h(t)$, can be calculated from the product of each signal in the frequency domain, $H(f)$ (i.e. product of their Fourier Transforms). As a consequence, the convolution of a time signal with itself is equal to the product of its Fourier Transform and its conjugate:

$$h(t)^* h(t) = H(f)H^*(f) = |H(f)|^2 \quad (5)$$

where the symbol * represents either the convolution operation or the conjugate of a complex variable. Using the Convolution Theorem and the similarities between the time-averaged auto-correlation function and the auto-convolution of the interface signal, it is possible to prove mathematically that the auto-correlation of a finite sample is estimated following these steps: (1) computation of the FFT of the treated time-series data; (2) computation of the square of the absolute value of the FFT; (3) application of the inverse FFT (IFTT) on the result and division by the total number of data points in the signal (see Auñón and Chandrasekar, 1997). These operations lead to the complete auto-correlation function estimate of the oil–water interface data.

Following the above approach, the auto-correlation function of the oil–water experimental data obtained in this work can be estimated by only using the FFT algorithm extensively. However, the procedure is not free from pitfalls and introduces spurious effects that need to be accounted for. The first one is the so-called *circular convolution problem* (Auñón and Chandrasekar, 1997; Bendat and Piersol, 2010). The FFT applied to the record treats the data as a periodic sequence of period T (i.e. 240 s). As a result, only the first period has the real data, while subsequent periods are repetitions of the same data. For a given delay, τ, it is clear that there is a collection of times, t, where signal values $x(t+\tau)$ belong to the original record (i.e. $t+\tau < T$); while at other times, t', signal values $x'(t'+\tau)$ fall out of the original record. As a consequence, the function computed via the FFT is not composed just of values $R_h(\tau)$. The procedure to avoid the circular problem consists of adding zeros at the end of the time record of the signal and prior to any computation (zero padding). In this investigation 69,632 zeros have been added for the record to have a total size of 2^{17}. The effect of doubling the size of the record is to avoid completely the problem. However, the auto-correlation function of the oil–water interface signal in this investigation generally decays quite fast (i.e. after about 0.5 s) and, in this case, the circular problem is not very important. In fact, the zero-padding was found not to have any effect on the auto-correlation function of the oil–water interface signal.

The second effect is the excessive noise introduced in the power spectrum by the auto-correlation estimate (i.e. non-smooth, rugged profile). This effect makes difficult the analysis of the spectrum. Fig. 3a shows the typical auto-correlation estimate of a stratified oil–water interface signal. The function decays rapidly and fluctuates around 0 after around 0.5 s. These fluctuations are seen to affect the final spectrum by making it significantly noisier without providing additional useful information. To avoid this, a truncation operation can be performed that uses a window function (Fig. 3b), according to which all the values of the auto-correlation estimate are set to 0 after 0.5 s and those before are modified by a cosine operation. The window function is applied to the estimate of the auto-correlation function prior to the final FFT. In this way, the spectrum is smooth as a result of the convolution of the auto-correlation and the window (Auñón and Chandrasekar, 1997). A cosine, Hamming window function was used in the current work (Harris, 1978). Fig. 4a and b shows the smoothing effect that this approach has on the final spectrum.

In summary, the following steps are followed to estimate the power spectrum of the conductivity probe signal from stratified wavy oil–water flows:

(a) Raw data is treated to remove trends and compensate for temperature and water salinity variations.
(b) The discrete time-series record is extended with the proper number of zeros. The total number of data points must be a power of 2. In this investigation, zeros are added up to a total number of 2^{17} data points.
(c) The FFT of the record is computed.
(d) The absolute value of the resulting FFT squared is computed.
(e) The IFFT (inverse Fourier Transform) is computed. The auto-correlation function is the IFFT divided by the total number of data-points (i.e. 2^{17}). The result gives the complete auto-correlation function. Since the second-half of the data-points is the mirror image of the first one, in practice, only the first 61,440 data points of the record can be taken (i.e. 240 s).
(f) The Hamming window is applied to the auto-correlation estimate with a time delay of 0.5 s.

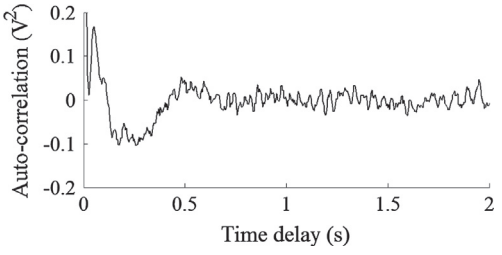

(a) Without Hamming truncation

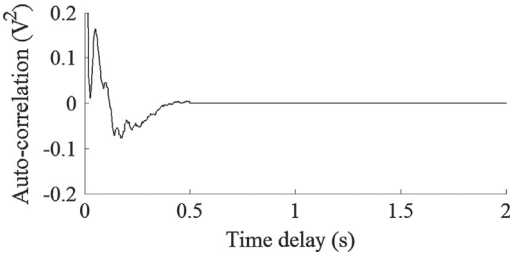

(b) With Hamming truncation ($\tau = 0.5$ s)

Fig. 3. Estimate of the auto-correlation function (U_{mix} = 1.33 ms^{-1}, r = 0.81).

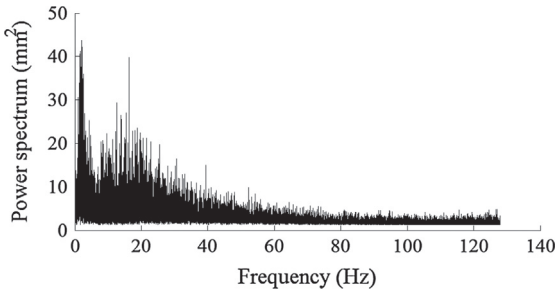

(a) Without Hamming truncation

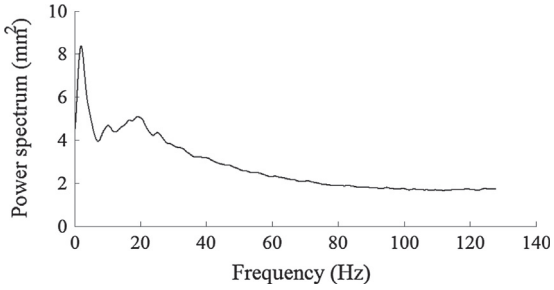

(b) With Hamming truncation ($\tau = 0.5$ s)

Fig. 4. Power spectrum estimate via Wiener–Khinchine theorem (U_{mix} = 1.33 ms^{-1}, r = 0.81).

(g) The FFT of the autocorrelation function, after applying the window, is computed. The absolute value is the two-sided spectral density estimate of the oil–water interface signal. As only positive frequencies have meaning, the resulting vector is multiplied by 2 to find the one-sided power spectrum (Bendat and Piersol, 2010). Since the spectrum is a mirror image with respect to the Nyquist frequency, only the first half of the one-sided spectrum is taken.

4. Results and discussion

Three main flow patterns were identified from visual observations and high speed imaging of the oil–water flows through the acrylic pipe as can be seen in Fig. 5. In stratified flow both phases retain their continuity and flow completely separately. This pattern occurs at mixture velocities, U_{mix}, lower than 1.4 ms^{-1} and oil-to-water input flow rate ratios, r, from 0.5 and 2.5. In dual-continuous (Dual-C.) flow both phases are continuous and a clear interface is visible, but regular drops of one phase (of variable size) flow along the pipe into the other phase. This pattern appears at large mixture velocities (above 2.1 ms^{-1}) for any input ratio, but also at lower mixture velocities if the input ratio is sufficiently different from 1 (either $r < 1$ or $r > 1$). Interestingly, for input ratio different from one, waves develop at the test section inlet regardless of the mixture velocity. On the contrary, at input ratios, r, around 1, no waves are seen at the inlet, even at high mixture velocities (see Fig. 6a and b, for $r > 1$ and $r = 1$, respectively). In all cases, downstream the test section small three dimensional fluctuations are present at the interface but no easily identifiable waves. Fig. 7 shows a typical photograph of the flow downstream the pipe. Above U_{mix} = 1.4 ms^{-1} and r around 1 the intermediate pattern is observed, where the flow is still stratified but with a rough interface and sporadic, small drops of one phase flowing into the other. The double lines in Fig. 5 mark the approximate boundaries between the different patterns. The flow regimes, the map and some photographs of the patterns have been discussed previously (Barral and Angeli, 2013).

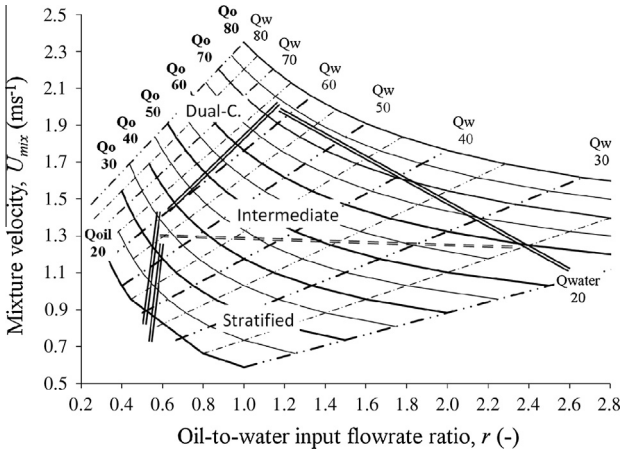

Fig. 5. Experimental flow pattern map.

A large number of different experimental oil–water flows were tested in the stratified regime. Some flows in the intermediate and dual-continuous patterns were also analyzed. In general, conductance probes and the methods used to compute the power spectrum or the time-averaged parameters of oil–water flows (Barral and Angeli, 2013) should not be used for the dual-continuous pattern, as the presence of drops affects the signal and introduces deviations in the expected results. The method and the probes can be used though in the intermediate regime where there are only very few drops present. As detailed in Section 2.1, two locations along the test section were investigated: immediately after the inlet (Position 1), where waves develop if the input ratio is different from 1; and 7 m downstream the inlet (~180 D, Position 2), where clear wave structures are not easily identifiable (Fig. 7) regardless of the input ratio.

4.1. Validation of the spectrum estimate

With the purpose of validating the estimates of the power spectrum via the procedure detailed in Section 3.3, the different oil–water flow rate combinations used were tested repeatedly at different days, sometimes months apart. It was found that the results are repeatable. Table 1 compares results obtained for two almost identical, stratified oil–water flows at $r < 1$ (U_{mix} = 0.77 and r = 0.7) and at $r > 1$ (U_{mix} = 0.85 ms^{-1} and r = 1.65) and Fig. 8a and b shows their respective spectra. The 2 mm probe was used to collect this data downstream the pipe (Position 2). The average interface height, h_i, the actual velocities of the two phases, U_o and U_w (calculated as shown in Barral and Angeli, 2013) and the average power of the spectrum are given in Table 1. The table and figures illustrate the level of reproducibility that can be achieved.

The average power of the spectrum offers a straightforward way to validate the power spectrum estimate. Eq. (1)can be inverted to:

$$R_h(\tau) = \int_{-\infty}^{+\infty} S(f) e^{i2\pi f\tau} df \tag{6}$$

In the special case of no time delay, $\tau = 0$, Eq. (6)becomes:

$$R_h(0) = \int_{-\infty}^{+\infty} S(f) df = E[h(t)^2] \tag{7}$$

which is the most general definition of the auto-correlation function for $\tau = 0$: the expectation, $E[\,]$, of the time-series data squared (i.e. moment of order 2 of the data). It is common to refer to the quantities in Eq. (7) as the average power of the random process (Auñón and Chandrasekar, 1997). Once an estimate of the spectrum has been found, Eq. (7)must be satisfied, thus validating the

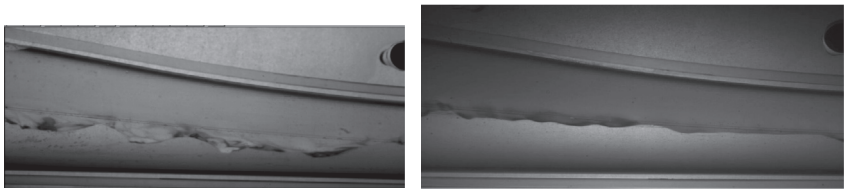

(a) $r = 2.5$ ($U_{mix} = 1.1$ ms^{-1}) **(b)** $r = 1$ ($U_{mix} = 2$ ms^{-1})

Fig. 6. Oil–water interfacial waves at the inlet section.

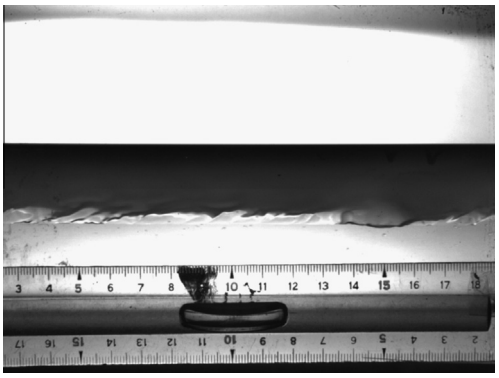

Fig. 7. Typical oil–water interface downstream ($r > 1$).

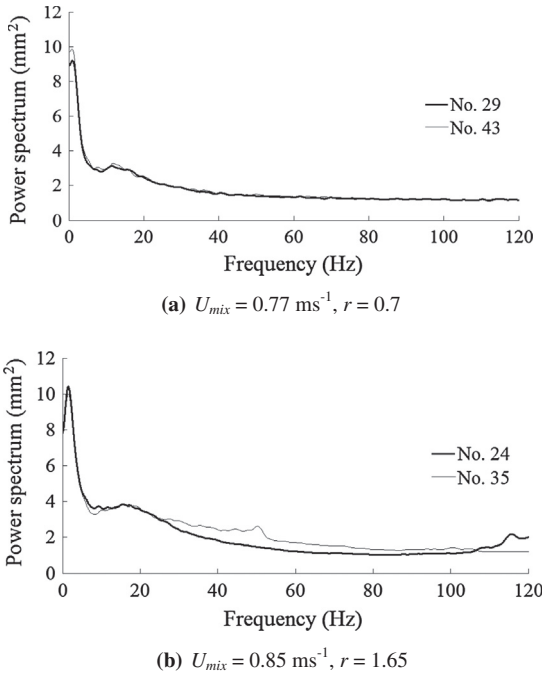

(a) $U_{mix} = 0.77$ ms^{-1}, $r = 0.7$

(b) $U_{mix} = 0.85$ ms^{-1}, $r = 1.65$

Fig. 8. Power spectra of the same oil–water flow rates collected at different days.

procedure. In practice, the average power found in this investigation from the auto-correlation and from the expectation of the time-series data was exactly the same. When computed from the spectrum estimate (middle term in Eq. (7)), it was usually within 5% of that value, although it was 10% different or slightly more in about 10–12% of all cases.

The signal collected from the conductance probes is typically affected by variations of water temperature and salinity. It can be seen from inspection of Eq. (7)that the average power of the signal is expected to be affected by such variations. To overcome the variations, all data was corrected against a calibration curve, as described in Barral and Angeli (2013). In this way, data collected in different occasions (i.e. days) could be compared using the same calibration base as a reference. However, in the course of this investigation, different calibrations were performed, usually every 2 months, or perhaps more frequently, typically after assembling/disassembling or cleaning the test section. It must be noted that two different calibrations are in general not identical. Therefore, care was taken not to compare data obtained under different calibration bases. An example of the differences in the average power of the same oil–water flow rate combinations but obtained under different calibration bases can be seen in Fig. 9a and b. All the data was collected with the 2 mm probe in Position 2. In both cases the lines from different calibration bases are roughly parallel for most part of the spectrum: the average power is seen to be different by 20% and 50% in Fig. 9a and b, respectively. It must be emphasized that the results discussed in the following sections are based on data belonging to the same "calibration campaign", and that cross-comparisons have been carefully avoided.

By comparing data having the same calibration curve, a trend was found between the average power and the mixture velocity. As can be seen in Fig. 10a, in stratified flow (up to $U_{mix} = 1.4$ ms^{-1}) the average power increases slightly with the mixture velocity. In intermediate flow (see Fig. 10b), however, the power is significantly larger and remains more or less constant. There seems to be a sharp increase in the value of the average power around $U_{mix} = 1.4$ ms^{-1}. In all cases, the oil-to-water input ratio does not play a significant role. The findings indicate that there is a direct relation between the average power of the data and the waviness of the interface seen with the high speed imaging and agrees with the observation of an intermediate region as a separate pattern characterized by a very rough interface.

Table 1
Comparison of two similar oil–water flows (29–43 and 24–35) obtained with the 2 mm probe located at 7 m from the inlet (Position 2).

Exp. No.	U_{mix} (ms^{-1})	r	h_i (mm)	U_o (ms^{-1})	U_w (ms^{-1})	Average power (mm^2)
29	0.78	0.69	20.58	0.83	0.86	1.68
43	0.76	0.68	21.48	0.86	0.80	1.71
24	0.84	1.63	14.73	0.91	0.92	1.91
35	0.84	1.67	14.62	0.92	0.91	2.08

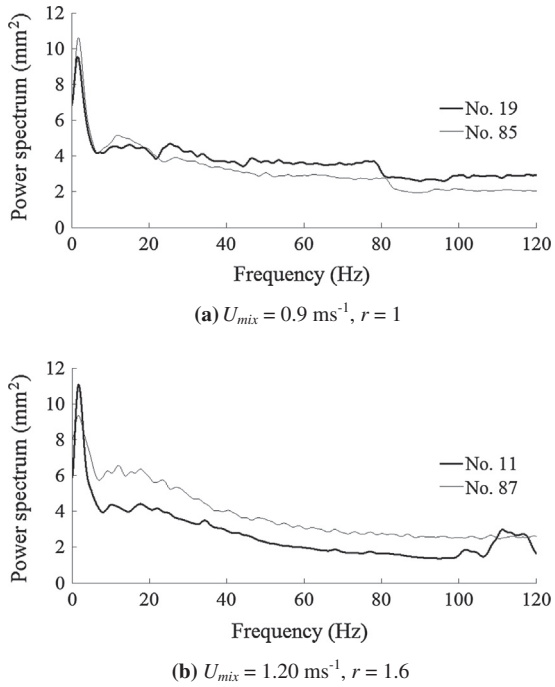

Fig. 9. Power spectra of the same oil–water flow rates collected at different experimental campaigns.

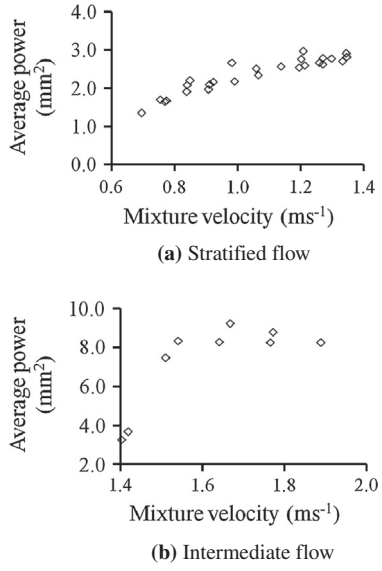

Fig. 10. Average power of the spectrum against mixture velocity (2 mm probe, Position 2).

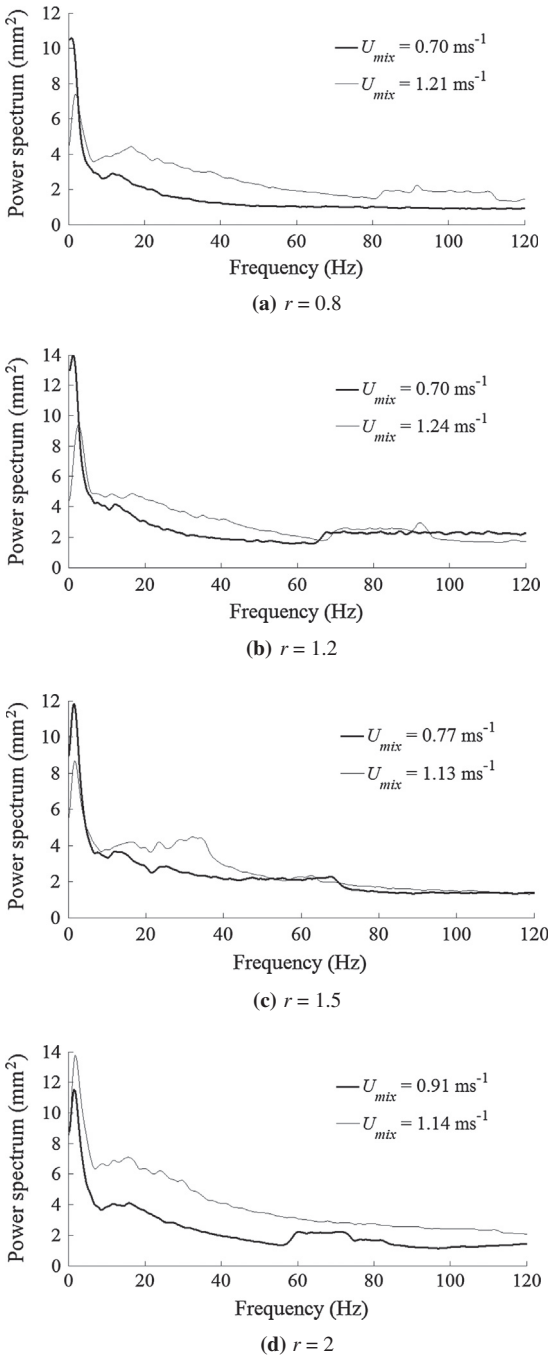

Fig. 11. Effect of mixture velocity on the power spectrum at different oil-to-water input ratios (2 mm probe, Position 2).

4.2. Influence of the mixture velocity on the spectrum

The influence of the mixture velocity has been investigated at different input ratios, *r*. Results, obtained with the 2 mm probe at Position 2 are shown in Fig. 11a–d as pairs of the same input ratio, *r* = 0.8, 1.2, 1.5 and 2, but with different mixture velocities. Comparisons are made with pairs of data that have the same calibration curve.

The graphs reveal that the power increases generally for most of the frequencies of the spectrum as the mixture velocity increases except from the peak at the 2–3 Hz, which tends to lose importance at higher mixture velocities. As a consequence, the average power tends to be higher with increasing mixture velocity. The redistribution of power with increasing velocity is not uniform, however, and the power in the range of frequencies 10–30 Hz increases more compared to the rest. On the contrary, spectra seem to be largely unaffected by mixture velocity very close to the inlet, where easily identifiable waves are clearly observed.

4.3. Contributing frequencies

It has been verified that the pumps induce mechanical vibrations in the experimental facility (Barral and Angeli, 2013). This contribution is a characteristic peak at about 2–3 Hz which tends to dominate over all other frequencies, especially at low mixture velocities (Fig. 11). These results seem to suggest that, at low

mixture velocities, the structure of the interface could almost entirely be described by external factors as, for example, induced mechanical vibrations, in the absence of any other disturbances. For signals collected in Position 2, there are two other ranges of frequencies with increased power compared to the rest of the spectrum. These are the frequencies between 10 and 30 Hz (that carry typically 40% of the maximum 2–3 Hz peak value), and larger frequencies, typically important at > 60 Hz (that carry about 25% of the maximum peak value). The range of frequencies between 10 and 30 Hz corresponds to the frequencies of the large waves seen at the inlet, which were verified from high speed video images by measuring the time elapsed between two consecutive waves crossing a fixed location on the image. The frequencies of at least 20 waves along the inlet were measured for 25 different flow rate combinations, ranging from $r = 0.4–3.5$ and $U_{mix} = 0.85–2$ ms^{-1}. In all cases frequencies at the inlet were found in the range 11–20 Hz . Even when no distinct waves are identified downstream the pipe, those frequencies remain in the fluid. The range of higher frequencies (> 60 Hz) is in agreement with the fluctuations seen at the oil–water interface downstream the test section (Fig. 7), which increase with mixture velocity. These frequencies though could also be affected by the data acquisition system.

To facilitate the study of the changes in these frequencies with flow conditions both groups are substituted by *weighted averages*, calculated as follows:

$$f_r = \frac{\sum_{i=a}^{b} f_i p_i}{\sum_{i=a}^{b} p_i} \tag{8}$$

where f_r is the representative frequency of the group; f_i is each individual frequency within the range of interest a–b (i.e. $a = 10$ Hz, $b = 30$ Hz or $a = 60$ Hz, $b = 100$ Hz); and p_i is the power of frequency f_i in the spectrum. When all the frequencies in a group have approximately the same power, Eq. (8) becomes the arithmetic mean.

For oil–water flow rate combinations within the stratified regime the weighted frequencies found are always the same, 19.4 ± 2.5% Hz for the first group and 79.3 ± 2.5% Hz for the second. These average frequencies do not seem to depend on mixture velocity or input ratio. Although the average frequencies seem to be independent of the flow conditions downstream the pipe, their importance within the spectrum increases with the mixture velocity. To demonstrate this, the power of the nearest frequency of the spectrum is attributed to the average frequency. This approximation is acceptable since the resolution of the spectrum is high compared to the precision of the frequencies shown here (i.e. 4.17×10^{-3} Hz, which is 1/240 s, against 19.4 Hz). The increase in the weighted frequency with mixture velocity for both frequency groups is seen in Fig. 12a and b, where the power of the frequency is given as a percentage of the power of the maximum peak of the spectrum at 2–3 Hz. The decrease in the power of the maximum peak with mixture velocity will tend to enhance the trend seen in Fig. 12a and b. Again, no trend is seen against the oil-to-water input ratio.

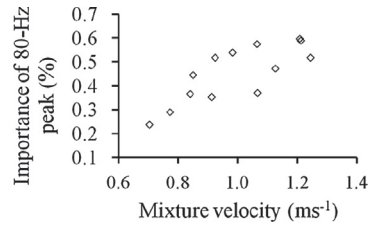

(a) 19-Hz peak

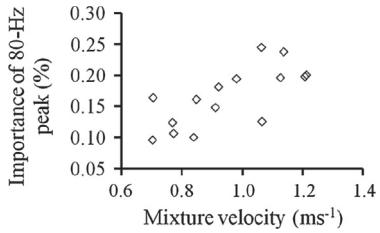

(b) 80-Hz peak

Fig. 12. Effect of mixture velocity on the relative importance of the frequencies at 19 Hz and at 80 Hz in the spectrum (2 mm probe, Position 2).

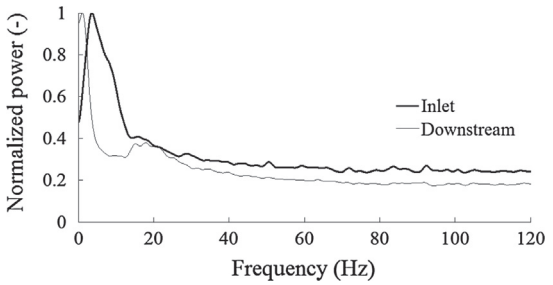

(a) $U_{mi} = 0.81$ ms^{-1}, $r = 0.57$

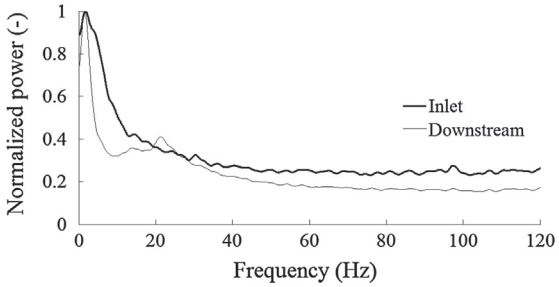

(b) $U_{mi} = 0.96$ ms^{-1}, $r = 0.63$

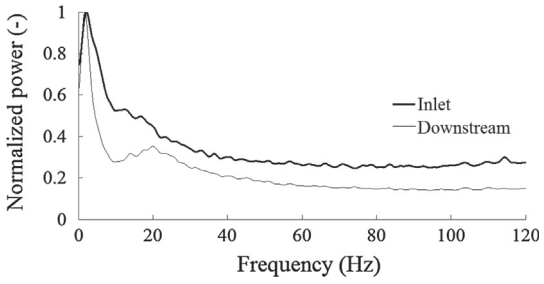

(c) $U_{mi} = 1.10$ ms^{-1}, $r = 0.67$

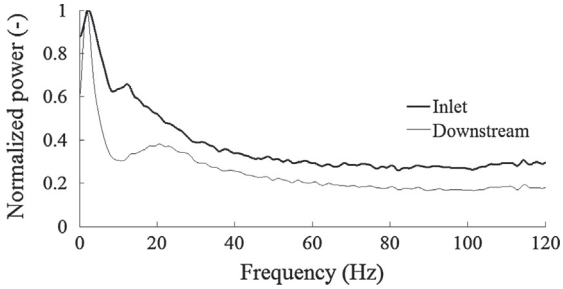

(d) $U_{mi} = 1.25$ ms^{-1}, $r = 0.70$

Fig. 13. Comparison of the power spectra of the flows near the test section inlet and at 7 m downstream for $r < 1$.

4.4. Comparison of power spectra near the inlet of the test section and at 7 m downstream

Interestingly, the same representative frequencies have been obtained when analyzing the data collected close to the test section inlet. In particular, the weighted frequency of 19 Hz is always computed at the inlet regardless of the mixture velocity and for both input ratios $r < 1$ and $r > 1$. The spectra of several oil–water flows at the inlet (Position 1) are compared to those at 7 m downstream the inlet (Position 2) in Fig. 13a–d and Fig. 14a–d for $r < 1$ and $r > 1$, respectively. Data was collected simultaneously in both locations, using the 5 mm probe at the inlet and the 2 mm one downstream. In order to compare the data collected from the two probes, the normalized power, found by dividing the power values with the maximum value, is used. The data indicate that contributing frequencies do not depend on the mixture velocity, although at Position 2 the relative importance of the contributing frequencies generally increases with the velocity at the expense of the pump contribution.

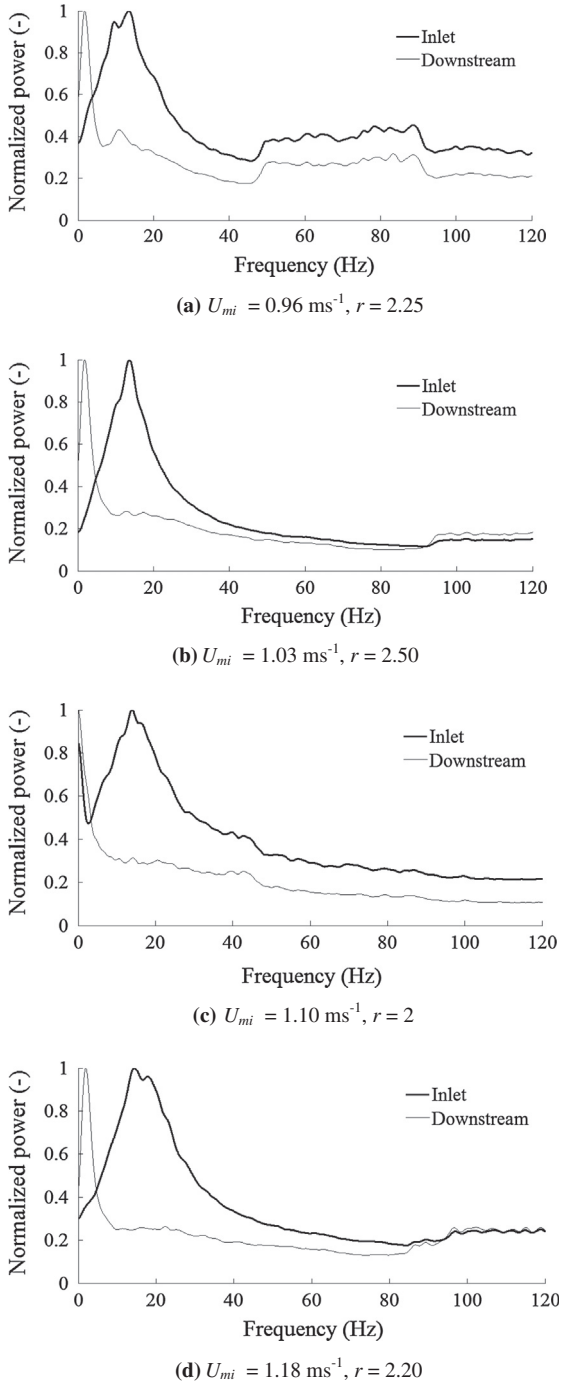

Fig. 14. Comparison of the power spectra of the flows near the test section inlet and at 7 m downstream for $r > 1$.

As can be seen in Fig. 13, for $r < 1$ the 19 Hz peak is not clearly seen in the spectra taken at the inlet and the low frequency contributions occur over a wide range. Downstream the pipe, however, the 19 Hz peak is clearly separated from the one due to mechanical vibrations. In contrast, for $r > 1$ (Fig. 14) the 19 Hz contribution in the spectra at the inlet is more prominent than for $r < 1$ and is comparable to that at 2–3 Hz. This difference is attributed to the geometry of the inlet. At input ratios $r < 1$ (water flow rate higher than that of the oil) the interface height is close to the upper pipe wall. The waves that develop on the interface are seen to collapse against the top wall shortly after the inlet junction as they enter the test section. This would reduce the wave amplitudes and may have an effect on the signal of the probe in Position 1, which is located a few centimeters away from the inlet junction. At 7 m downstream the inlet (Position 2) and for both input ratios the main peak is that of the pump while the peak at 19 Hz is still present but not as prominent. This finding agrees with the observation that almost two-dimensional waves develop at the inlet with large amplitudes at input ratios different from 1 (Fig. 6a); these waves reduce in amplitude significantly and acquire a complex three-dimensional configuration further downstream the pipe (Fig. 7). In both Figs. 13 and 14 the normalized spectra lines at the inlet are always above those at 7 m downstream, apart from the low frequency region (attributed to mechanical vibrations). This suggests that the importance of the contributing frequencies seen at the inlet diminishes downstream in favor of the low frequency due to mechanical vibrations. This is particularly obvious for the characteristic frequency at19 Hz. The fact that the 19 Hz frequency appears at all the different fluid flow rates tested suggests that it could be a characteristic of the system of the fluids used rather than the result of the flow conditions.

5. Conclusions

In this work, the power spectrum of the interface in stratified, horizontal oil–water flows was estimated from the signal of double wire conductance probes. Experiments were carried out at two locations, immediately after the test section inlet and at 7 m downstream the pipe. The main contributions of this work are summarized as follows:

(1) A complete methodology to compute the power spectrum of the oil–water interface was presented. The methodology is based on the extensive used of the Fast Fourier Transform (FFT) algorithm. The procedure is fast and readily applicable to stratified oil–water flows, as long as the signal properties of normality and stationarity are satisfied.
(2) In stratified flows, the average power of the spectrum increases with the mixture velocity. At the transition to the intermediate flow pattern there is a sudden large increase in the power values which reflects the interface roughness of that flow pattern.
(3) Two main contributing frequency ranges were identified in the stratified regime: at 2–3 Hz, attributed to the mechanical vibrations of the flow system, and at about 19 Hz. In addition, smaller contributions were found at a range of frequencies above 60 Hz. At fixed input oil to water flow rate ratio, the power of the 19 Hz frequency tends to increase with increasing mixture velocity.

(4) Spectra were compared between the inlet and the downstream test section locations. The 19 Hz contribution was found to be always present, regardless of the flow conditions. Generally, waves with frequency of 19 Hz are generated at the inlet at input ratios different from 1. As the fluids flow further downstream the 19 Hz frequency remains in the structure of the interface, but the amplitude of the corresponding waves decreases while small amplitude three-dimensional waves appear. Its importance in the spectrum is, thus, reduced.

Further investigations would be required to evaluate the effect of fluids properties on the frequencies observed. The relation between amplitudes of the frequencies in the spectrum with interfacial wave amplitudes also needs to be established.

Acknowledgements

The authors would like to thank Chevron Technology Company and UCL for their financial support. They are also grateful to the people of the Chemical and Biochemical Engineering workshop at UCL for manufacturing the probes and to Dr. Simon Barrass for technical support with the instrumentation.

References

Alamu, M.B., Azzopardi, B.J., 2011. Flow pattern and slug dynamics around a flow splitter. J. Fluids Eng. 133 (12), 121105.
Al-Wahaibi, T., Angeli, P., 2007. Transition between stratified and non-stratified horizontal oil–water flows. Part I: Stability analysis. Chem. Eng. Sci. 62, 2915–2928.
Al-Wahaibi, T., Angeli, P., 2011. Experimental study on interfacial waves in stratified horizontal oil–water flow. Int. J. Multiphase Flow 37 (8), 930–940.
Al-Wahaibi, T., Smith, M., Angeli, P., 2007. Transition between stratified and non-stratified horizontal oil–water flows. Part II: Mechanism of drop formation. Chem. Eng. Sci. 62, 2929–2940.
Andritsos, N., 1992. Statistical analysis of waves in horizontal stratified gas–liquid flow. Int. J. Multiphase Flow 18 (3), 465–473.
Auñón, J.I., Chandrasekar, V., 1997. Introduction to Probability and Random Processes. McGraw Hill.
Azzopardi, B.J., 1997. Drops in annular two-phase flow. Int. J. Multiphase Flow 23 (7), 1–53.
Bai, R., 1995. Traveling Waves in a High Viscosity Ratio and Axisymmetric Core Annular Flow. PhD Dissertation, University of Minnesota.
Bannwart, A.C., 1998. Wavespeed and volumetric fraction in core annular flow. Int. J. Multiphase Flow 24 (6), 961–974.
Barral, A.H., Angeli, P., 2013. Investigation of stratified, horizontal oil–water flow via statistical analysis of conductance probe data. Exp. Fluids 54 (10), 1604.
Bendat, J.S., Piersol, A.G., 2010. Random Data: Analysis and Measurement Procedures. Wiley, New Jersey.
Chakrabarti, D.P., Das, G., Das, P.K., 2006. The transition from water continuous to oil continuous flow pattern. AIChE J. 52 (11), 3668–3678.
Cooley, J.W., Tuckey, J.W., 1965. An algorithm for the machine calculation of complex Fourier series. Math. Comput. Model 19, 297–301.
De Castro, M.S., Pereira, C.C., Dos Santos, J.N., Rodriguez, O.M.H., 2012. Geometrical and kinematic properties of interfacial waves in stratified oil–water flow in inclined pipe. Exp. Therm. Fluid Sci. 37, 171–178.
Du, M., Jin, N.D., Gao, Z.K., Wang, Z.Y., Chen, P., 2012. Time–frequency analysis of vertical upward oil–water two-phase flow. Presented at the 7th international symposium on measurement techniques for multiphase flows. AIP Conf. Proc. 1428, 107–114.
Fossa, M., 1998. Design and performance of a conductance probe for measuring liquid fraction in two-phase gas–liquid flows. Flow Meas. Instrum. 9 (2), 103–109.
Harris, F.J., 1978. On the use of windows for harmonic analysis with the discrete Fourier Transform. Proc. IEEE 66 (1), 51–83.
Hernández, L., Juliá, J.E., Chiva, S., Paranjape, S., Ishii, M., 2006. Fast classification of two-phase flow regimes based on conductivity signals and artificial neural networks. Meas. Sci. Technol. 17 (6), 1511–1521.
Ishii, M., Grolmes, M.A., 1975. Inception criteria for droplet entrainment in two-phase concurrent film flow. AIChE J. 21 (2), 308–318.
Jin, N.D., Nie, X.B., Ren, Y.Y., Liu, X.B., 2003. Characterization of oil/water two-phase flow patterns based on non-linear time series analysis. Flow Meas. Instrum. 14, 169–175.
Jurman, L.A., Bruno, K., McCready, M.J., 1989. Periodic and solitary waves on thin, horizontal, gas-sheared liquid films. Int. J. Multiphase Flow 15 (3), 371–384.
Kim, S., Fu, X.Y., Wang, X., Ishii, M., 2000. Development of the miniaturized four-sensor conductivity probe and the signal processing scheme. Int. J. Heat Mass Transfer 43, 4101–4118.
Oliemans, R.V.A., 1986. The lubricating-film model for core-annular flow. PhD Dissertation, Delft University.
Panagiotopoulos, N., Lucas, G.P., 2007. Simulation of a local four-sensor conductance probe using a rotating dual-sensor probe. Meas. Sci. Thecnol. 18 (8), 2563–2569.
Rodriguez, O.M.H., Bannwart, A.C., 2006. Analytical model for interfacial waves in vertical core flow. J. Pet. Sci. Eng. 54 (3–4), 173–182.
Shannon, C.E., 1949. Communications in the presence of noise. Proc. IRE 37, 10–21.
Sun, B., Wang, E.P., Zhang, Y.J., 2011. Time-frequency spectral analysis of gas–liquid two-phase flow's fluctuations. Acta Phys. Sin. 60 (1), 014701.
Trallero, J.L., 1995. Oil–Water Flow Patterns in Horizontal Pipes. PhD Dissertation, University of Tulsa.
Tsochatzidis, N.A., Karapantsios, T.D., Kostoglou, M.V., Karabelas, A.J., 1992. A conductance probe for measuring liquid fraction in pipes and packed beds. Int. J. Multiphase Flow 18 (5), 653–667.
Wang, Z., Gabriel, K.S., Manz, D.L., 2004. The influences of wave height on the interfacial friction in annular gas–liquid flow under normal and microgravity conditions. Int. J. Multiphase Flow 30 (10), 1193–1211.
Wu, Q., Ishii, M., 1999. Sensitivity study on double-sensor conductivity probe for the measurement of interfacial area concentration in bubbly flow. Int. J. Multiphase Flow 25, 445–453.
Xu, W.F., Xu, L.J., Cao, Z., Chen, J.J., Liu, X.B., Hu, J.H., 2012. Normalized least-square method for water hold-up measurements in stratified oil–water flow. Flow Meas. Instrum. 27, 71–80.
Zhai, L., Jin, N., Zong, Y., Wang, Z., Gu, M., 2012. The development of a conductance method for measuring liquid hold-up in horizontal oil–water two-phase flows. Meas. Sci. Technol. 23 (2), 025304.